



Article

# Raman Imaging—A Valuable Tool for Tracking Fatty Acid Metabolism—Normal and Cancer Human Colon Single-Cell Study

Karolina Beton-Mysur , Monika Kopec and Beata Brozek-Pluska \*

Laboratory of Laser Molecular Spectroscopy, Institute of Applied Radiation Chemistry, Faculty of Chemistry, Lodz University of Technology, Wroblewskiego 15, 93-590 Lodz, Poland; karolina.beton@dokt.p.lodz.pl (K.B.-M.); monika.kopec@p.lodz.pl (M.K.)

\* Correspondence: beata.brozek-pluska@p.lodz.pl; Tel.: +48-42-631-31-92

**Abstract:** Altered metabolism of lipids is a key factor in many diseases including cancer. Therefore, investigations into the impact of unsaturated and saturated fatty acids (FAs) on human body homeostasis are crucial for understanding the development of lifestyle diseases. In this paper, we focus on the impact of palmitic (PA), linoleic (LA), and eicosapentaenoic (EPA) acids on human colon normal (CCD-18 Co) and cancer (Caco-2) single cells using Raman imaging and spectroscopy. The label-free nature of Raman imaging allowed us to evaluate FAs dynamics without modifying endogenous cellular metabolism. Thanks to the ability of Raman imaging to visualize single-cell substructures, we have analyzed the changes in chemical composition of endoplasmic reticulum (ER), mitochondria, lipid droplets (LDs), and nucleus upon FA supplementation. Analysis of Raman band intensity ratios typical for lipids, proteins, and nucleic acids ( $I_{1656}/I_{1444}$ ,  $I_{1444}/I_{1256}$ ,  $I_{1444}/I_{750}$ ,  $I_{1304}/I_{1256}$ ) proved that, using Raman mapping, we can observe the metabolic pathways of FAs in ER, which is responsible for the uptake of exogenous FAs, de novo synthesis, elongation, and desaturation of FAs, in mitochondria responsible for energy production via FA oxidation, in LDs specialized in cellular fat storage, and in the nucleus, where FAs are transported via fatty-acid-binding proteins, biomarkers of human colon cancerogenesis. Analysis for membranes showed that the uptake of FAs effectively changed the chemical composition of this organelle, and the strongest effect was noticed for LA. The spectroscopy studies have been completed using XTT tests, which showed that the addition of LA or EPA for Caco-2 cells decreases their viability with a stronger effect observed for LA and the opposite effect observed for PA. For normal cells, CCD-18 Co supplementation using LA or EPA stimulated cells for growing, while PA had the opposite impact.

**Keywords:** Raman spectroscopy; Raman imaging; fatty acids; colon cancer; metabolism; cancer biomarkers



**Citation:** Beton-Mysur, K.; Kopec, M.; Brozek-Pluska, B. Raman Imaging—A Valuable Tool for Tracking Fatty Acid Metabolism—Normal and Cancer Human Colon Single-Cell Study. *Int. J. Mol. Sci.* **2024**, *25*, 4508. <https://doi.org/10.3390/ijms25084508>

Academic Editor: Gabriella Calviello

Received: 27 March 2024

Revised: 14 April 2024

Accepted: 17 April 2024

Published: 19 April 2024



**Copyright:** © 2024 by the authors. Licensee MDPI, Basel, Switzerland. This article is an open access article distributed under the terms and conditions of the Creative Commons Attribution (CC BY) license (<https://creativecommons.org/licenses/by/4.0/>).

## 1. Introduction

Altered lipid metabolism is a key indicator of many diseases including cancer [1,2]. Therefore, this class of compounds is attracting growing interest as biomarkers in clinical applications, highlighting the role of lipidomics in cancer studies.

In this paper, we focus on lipid metabolism with special emphasis on fatty acids (FAs)—saturated (palmitic acid (PA, 16:0)) and unsaturated (linoleic acid (LA, 18:2) and eicosapentaenoic acid (EPA, 20:5))—and their potential in diagnostics and therapies of colorectal cancer (CRC).

Most often, CRCs are adenocarcinomas arising from pathological changes in the mucosa's epithelial cells [3]. Approximately 30% of CRCs are associated with hereditary gene mutations. Disfunctions of repair genes are responsible for around 15% of CRCs; the other 80–85% is associated with mutations in adenomatous polyposis coli gene (APC). Furthermore, CRCs may develop as a consequence of inflammatory bowel disease (IBD) [4]. Two of

the most common genetic defects found in CRCs are KRAS and p53 mutations. Moreover, it has been shown that these mutations are associated with enhanced proliferation of cancerous cells [5,6].

Evidence of lipid reprogramming metabolism in cancer cells was first reported in the 1920s, when the Warburg effect was described the first time [7]. However, nowadays, a shift towards the reversed Warburg effect is popular, since researchers proved that each type of cancer cell has unique metabolic features and some may synthesize ATP by means of oxidative phosphorylation [8]. The metabolic pathways of lipids that have been affected in CRC cells include, among others, the synthesis, desaturation, elongation, and mitochondrial oxidation of FAs.

Generally, lipids can be described as a diverse group of compounds. LIPID MAPS [9] classified them (based on the presence of isoprene and ketoacyl groups) as follows: FAs, sphingolipids, sterol lipids, glycerolipids, glycerophospholipids, prenol lipids, saccharolipids, and polyketides [10].

However, for the proper functioning of organisms, polyunsaturated fatty acids (PUFAs) are required. These acids are formed from palmitic acid (PA) as a result of the action of desaturases causing the introduction of a double bond into the structure of the acid molecule. From PA, palmitoleic acid (C16:1  $\omega$ -7) is formed, and from stearic acid, and oleic acid (OA, C18:1  $\omega$ -9) is formed. As a result of the action of  $\Delta$ 12-desaturase, oleic acid is converted to linoleic acid (LA, C18:2  $\omega$ -6), which is further converted by  $\Delta$ 15-desaturase to  $\alpha$ -linolenic acid (ALA, C18:3  $\omega$ -3).

However, in animal tissues, double bonds can only be introduced between the already existing double bond and the carboxyl group due to the lack of suitable desaturases. Therefore, the synthesis of LA and ALA does not take place in animal tissues, and they must be supplied in the diet [11].

The detailed description of FA biosynthesis and schematic presentation of FA biosynthesis is shown in Figure S1 provided in the Supplementary Materials (SM). Please see Figure S1 in the Supplementary Materials.

Figure 1 shows the correlation between the structure of FAs and formation of eicosanoids.

PA is a fatty acid with a 16-carbon chain. It is the most common saturated FA found in animals, plants, and microorganisms. In the human body, PA may participate in the regulation of hormone secretion as well as in the transmission of signals between body cells. PA may also support the proper functioning of the immune system [12]. However, it must be emphasized that the positive effect of this compound can be observed only for small doses of PA [13–15]. Contrarily, a high consumption of PA in the daily diet may have a negative impact on the human body, contributing to an increase in the concentration of total cholesterol in the blood serum and an increase in its LDL (low-density lipoprotein) fraction [16–19]. This, in turn, may increase the risk of atherosclerosis and cardiovascular diseases. Additionally, excessive consumption of saturated fatty acids (SFAs), including PA, may increase the risk of obesity and digestive disorders [20–22]. Many research groups have also proven the correlation between PA overconsumption and cancer development [23]. Through lipidomics analysis, Lin et al. demonstrated that PA can impact the aggressiveness of cancer cells. The authors highlighted the changes in cell membrane fluidity and glucose metabolism regulation [24]. Sun et al. demonstrated that PA may regulate the expression of genes involved in the metabolism of FAs, such as fatty acid synthase gene (FASN), stearoyl-CoA desaturase-1 (SCD1), and elongation of long-chain FA family member 6 (ELOVL6), which are directly associated with gastric cancer [25]. Zhang et al. investigated the impact of PA on the genes pyruvate dehydrogenase kinase 4 (PDK4) and ACSL5, which stimulate the proliferation of lung cancer cells [26]. Metastasis of cancer cells upon FA supplementation was also investigated by Pascual et al. [27]. Researchers conducted experiments on human oral squamous cell carcinoma (OSCC). They supplemented OSCC with PA, OA, and LA before injecting them into mice. The study revealed that pretreatment with PA, in contrast to OA or LA, significantly increased the formation of metastases. Notably, cells treated with PA showed metastatic properties even after PA removal for 2 weeks or treatment with OA.

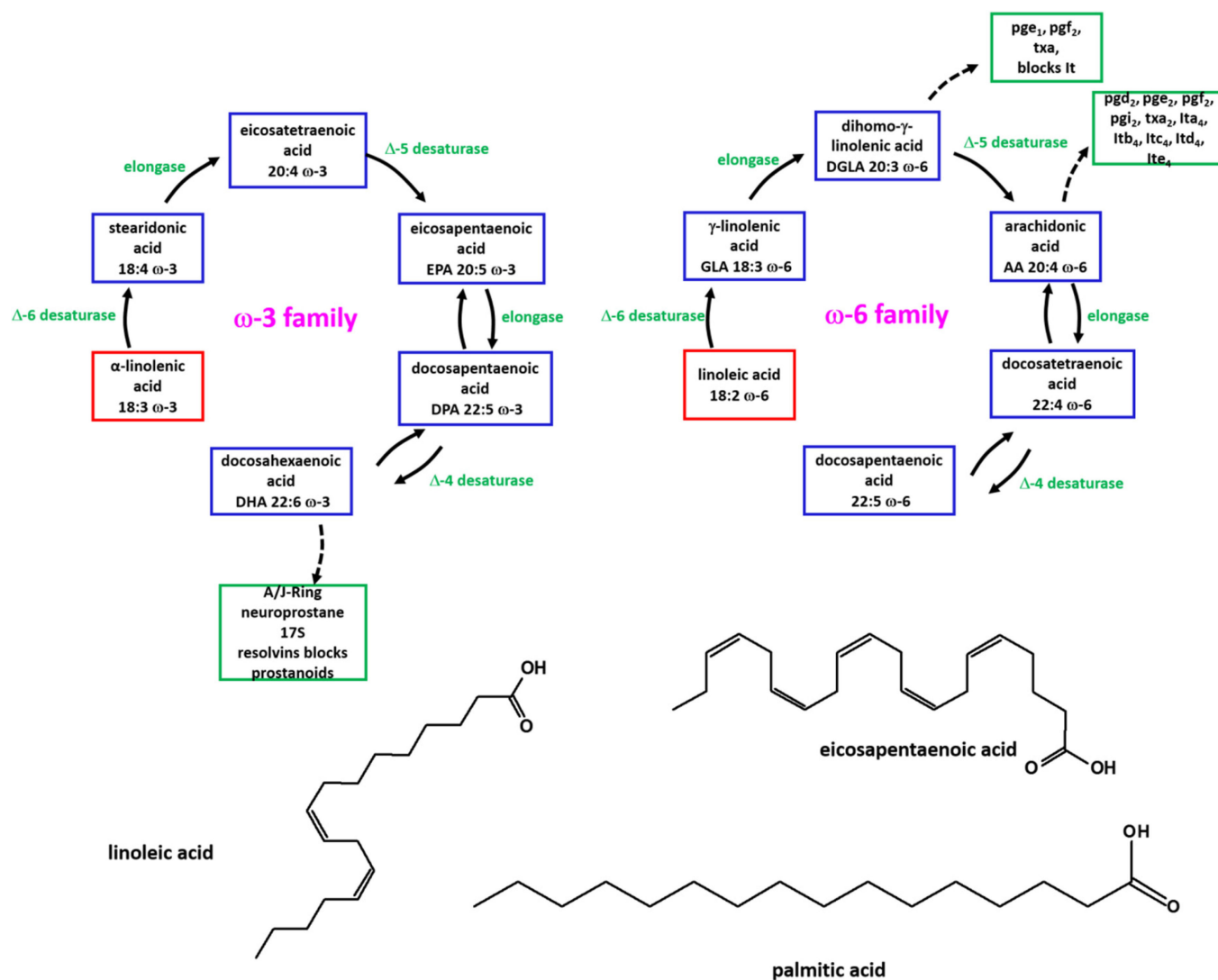


**Figure 1.** Schematic representation of formation of eicosanoids by  $\omega$ -3 and  $\omega$ -6 FAs.

Therefore, nutrition experts and medical doctors recommend replacing SFAs with essential unsaturated fatty acids (UFAs), the consumption of which can have beneficial effect on human health and positively affect the functioning of the body [28–31].

LA is a fatty acid with an 18-carbon chain, 2 double bonds and typically occurs as a triglyceride in nature rather than as a free FA. LA is one of two essential FAs for humans, and serves also as a precursor to arachidonic acid, which is a parent molecule for prostaglandins, leukotrienes, thromboxane, endocannabinoids and eicosanoids [32]. Large scale human epidemiological studies indicated that high intakes of LA protect against cancer development [33]. The first beneficial effect of CLA (conjugated LA) as anti-cancer agent was discovered by M. Pariza [34]. Synthetically prepared CLA isomers were applied by researchers to mice prior to the initiation of epidermal carcinomas. Mice that received CLAs developed only half the number of papillomas [35]. Subsequent studies have proved also that other murine carcinoma models show an improvement with CLA supplementation, including mammary [36], colon [37], stomach [38] and prostate cancers [39].

EPA is a fatty acid with a 16-carbon chain and 5 double bonds, and is a precursor for prostaglandin-3, thromboxane-3, and leukotriene-5 eicosanoids. EPA is also both a precursor and a hydrolytic breakdown product of eicosapentaenoyl ethanolamide [40]. Bie et al. have shown that EPA attenuates ovarian cancer by improving immunomodulation. The immunomodulatory effects of EPA were associated with PI3K/Akt, ERK1/2 and NF-

$\kappa$ B P65 expression [41]. Moreover, Ando et al. proved that EPA suppresses angiogenesis by reducing the secretion of IL-6 and VEGF from colon-cancer-associated fibroblasts [42]. It has also been shown that EPA decreases systemic inflammation caused by IL-6 [43] and decreases inflammation caused by cancers [44].

Visualizing the presence and distribution of fatty acids within cells, both in their free and esterified forms, is crucial for comprehending how these molecules are integrated, stored, and processed. However, existing techniques for imaging multiple intracellular fatty acids have been hindered by their minute size, posing challenges in labeling and tracking without altering their essential biological and biophysical properties. Here, we introduce a novel approach for visualizing intracellular fatty acids and their accumulation within specific cell organelles. Leveraging distinct Raman spectra associated with different labeling patterns, our Raman imaging technique enables the identification and tracking of fatty acids within cells. Our findings reveal that fatty acids with a higher double bond content tend to accumulate more prominently within endoplasmic reticulum and lipid droplets. This innovative methodology not only sheds light on the spatial dynamics of fatty acids but also holds promise for elucidating the behavior of various other metabolites within cells. Research into the detection of fatty acids, their storage sites or the tracking of fat metabolism products has been successfully carried out by various research groups from around the world. Lipid metabolism and its mechanism have been the subject of research by scientists from all over the world; however, Raman spectroscopy is a unique method in this aspect as it gives very precise, unambiguous results, allowing the registration of even the smallest changes occurring in the cell as a result of fatty acid supplementation [45–53].

In summary, an increased incidence of cancers (including CRCs) is typical among people consuming a larger amount of animal saturated fats, with a diet rich in myristic, lauric, and palmitic acids. In contrast, a reduction in morbidity under the influence of ALA, DHA, and EPA was observed in relation to stomach [54], pancreas [55,56], colon [57,58], lung [59], breast [60,61], and prostate cancer [62]. Figure 2 shows the simplified metabolic pathways in normal and excess dietary fat with an increased or balanced SFA/PUFA ratio.

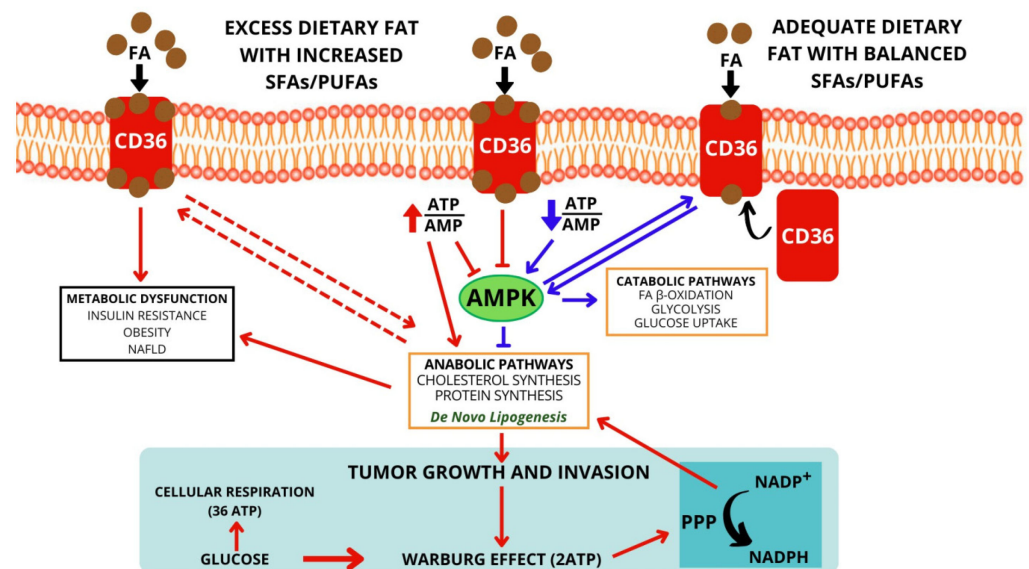


**Figure 2.** Metabolic pathways in normal and excess dietary fat with increased or balanced SFA/PUFA ratio.

All of the aforementioned factors confirm the crucial role of FAs in human body homeostasis and provide compelling topics for new investigations. In this paper, we focus on the impact of PA, LA, and EPA on human colon single cells using Raman imaging and spectroscopy. The spectroscopy studies were completed with XTT tests analyzing the viability of normal CCD-18 Co and cancer Caco-2 human colon cells upon FA supplementation.

## 2. Results

The uncontrolled cellular growth typical of cancer development requires a constant supply of nutrients. The most crucial role in an unbalanced diet stimulating tumors growth is played by sugars and fats. Since the 1970s, numerous studies proved the adverse impact of sugars and fats on human health including increased cancer risk [63]. There is convincing evidence that excess body weight is associated with an increased risk for many cancers including endometrial, esophageal, hepatocellular carcinoma; renal and pancreatic adenocarcinomas; gastric cardia cancer; meningioma; multiple myeloma; and colorectal, postmenopausal breast, ovarian, gallbladder and thyroid cancers [64].

To identify the impact of FAs on human colon cells, we established a single-cell analysis approach, which, in the first step, couples the analysis of Raman maps and mean single Raman spectra. To properly address biochemical changes, with the main focus on the metabolism of FAs in human normal and cancer colon cells upon FA supplementation in comparison to not supplemented types, we systematically investigated how the Raman method responds to in vitro samples. We used spontaneous Raman spectroscopy to record vibrational spectra and Raman maps at the single-cell level for human colon cell lines: CCD-18 Co (normal) and Caco-2 (cancer) over the molecular spectral range of 500–1800  $\text{cm}^{-1}$  (the fingerprint region).

Figure 3 shows the Raman data obtained for human colon normal cells (CCD-18 Co) including cells upon EPA supplementation (for transparency of data presentation, we show the data for one cell). The data for Caco-2 human colon cancer cells including the EPA-supplemented type are presented in Figure 4. Data for LA supplementation are presented in Figure S3 (for CCD-18 Co line) and Figure S4 (for Caco-2 line), and data for PA supplementation are shown in Figure S5 (for CCD-18 Co line). Each figure contains panels presenting intensity spectra with an interpretation of individual components and assignment to individual cellular organelles, which we explain in the Section 3.

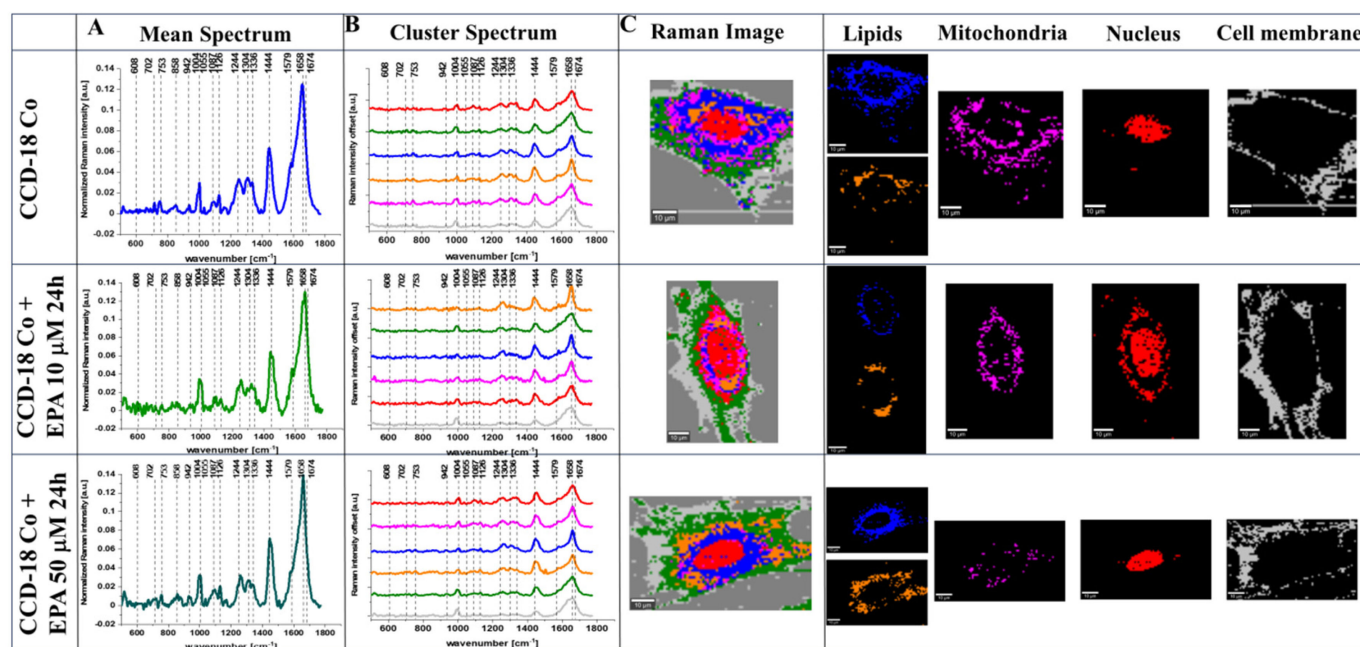


**Figure 3.** The mean Raman spectra for cells as a whole (A), the mean Raman spectra typical for all clusters identified by using cluster analysis (CA) (B), Raman images constructed based on CA (C), and the single clusters wherein blue and orange correspond to lipid rich regions, magenta corresponds to mitochondria, red corresponds to nucleus, and gray corresponds to cell membrane identified by using CA for human normal colon cells CCD-18 Co without any supplementation and upon EPA supplementation for 24 h, for 10  $\mu\text{M}$  and 50  $\mu\text{M}$ . All cells were measured in PBS. The scale bar represents 10  $\mu\text{m}$ . Colors of the spectra correspond to the colors of clusters.

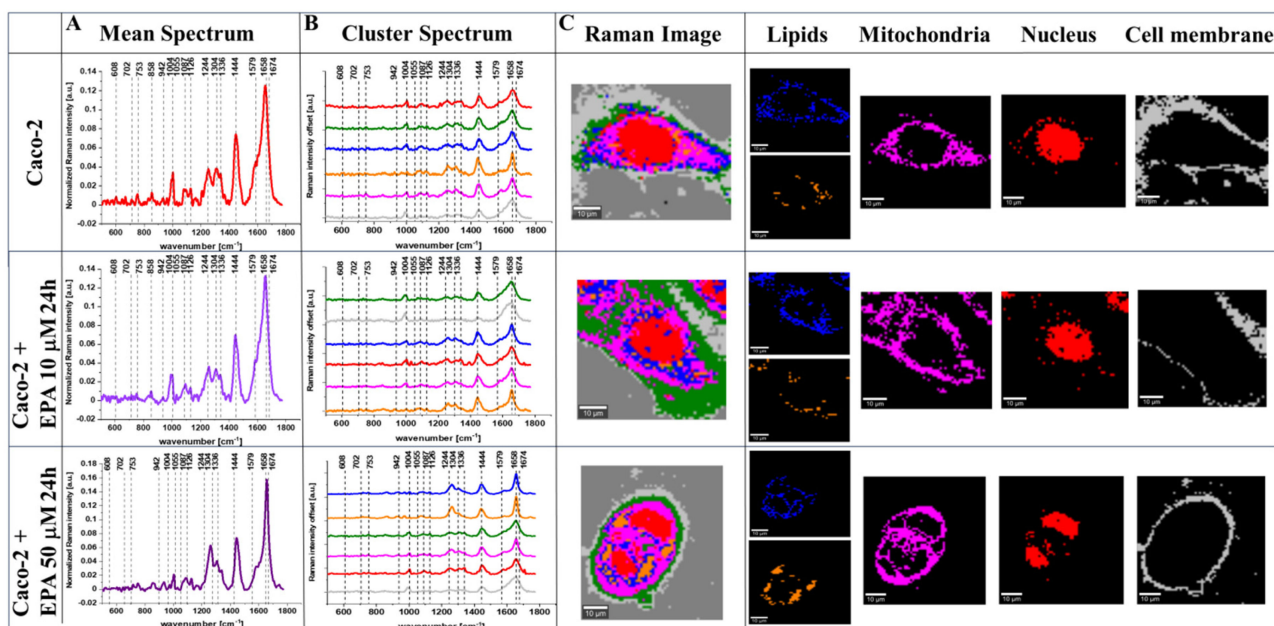


**Figure 4.** The mean Raman spectra for cells as a whole (A), the mean Raman spectra typical for all clusters identified by using cluster analysis (CA) (B), Raman images constructed based on CA (C), and the single clusters wherein blue and orange corresponds to lipid rich regions, magenta corresponds to mitochondria, red corresponds to nucleus, and gray corresponds to cell membrane identified by using CA for human colon cancer cells Caco-2 without any supplementation and upon EPA supplementation for 24 h, for 10 μM and 50 μM. All cells were measured in PBS. The scale bar represents 10 μm. Colors of the spectra correspond to the colors of clusters.

The results for LA and PA are presented in Figures S3–S5 in the Supplementary Materials.

One can see from Figures 3, 4 and S3–S5 that Raman imaging (RI) can be used to obtain detailed information regarding the subcellular structure of each type of human colon cell: normal, cancer, and normal or cancer upon FA supplementation. Based on CA, which is a well-established method for RI data elaboration [65], we have identified, for each cell: the endoplasmic reticulum (ER, blue), the lipid droplets (LDs, orange), the cytoplasm (green), the nucleus (red), the mitochondria (magenta), and the cell membrane (gray). Moreover, Raman spectroscopy allowed us to obtain well-resolved vibrational spectra based on which one can identify the main chemical compounds: nucleic acids, lipids, proteins, saccharides, etc.

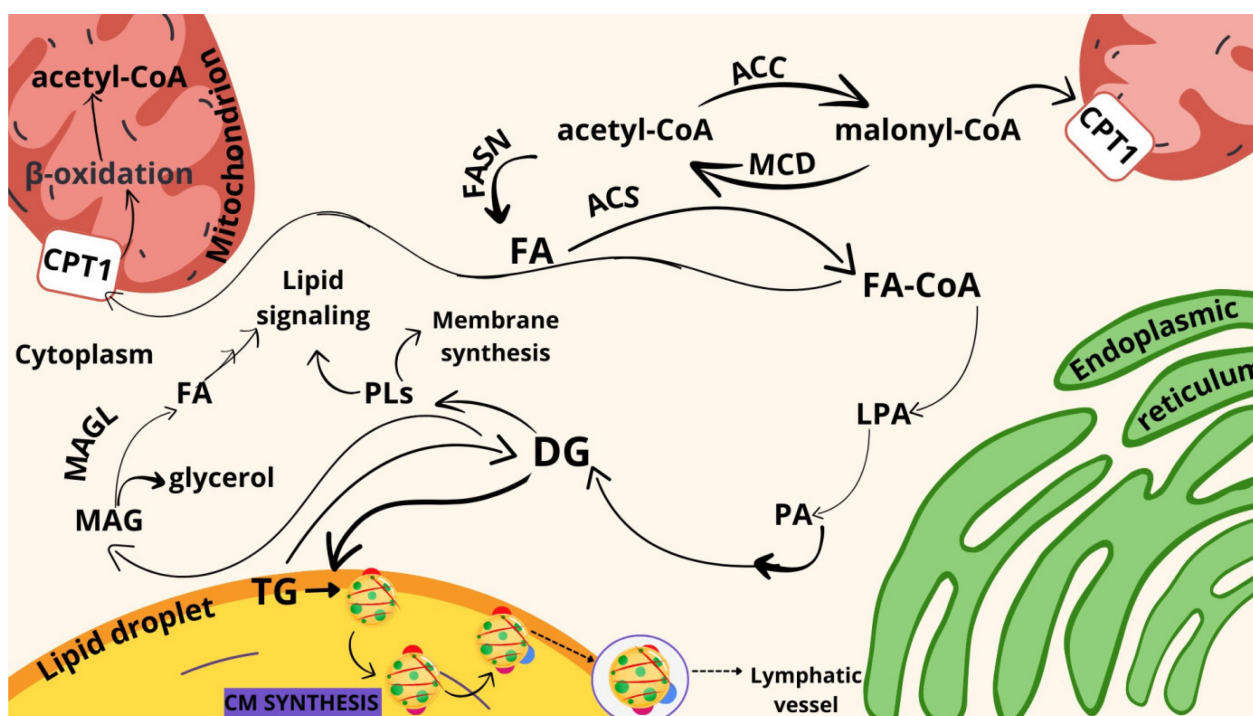
The usefulness of RI for single-cell analysis at the level of individual organelles has been proven in our previous papers [66–69]. Moreover, fluorescence staining confirmed the effectiveness of RI for individual structure visualization and correctness of Raman data interpretation [70–75]. Scheme S1 in the Supplementary Materials shows the simplified illustration of the RI experiment idea and the comparison of RI and fluorescence data for one cell chosen from our database.

Lipidomics studies are so important because altered lipid metabolism has been observed for drug resistance; e.g., increased *de novo* lipogenesis mediated by FAS facilitated gemcitabine resistance in pancreatic cancer [76]. Moreover, it has been shown that the cancer-associated adipose tissue promoted resistance to anti-angiogenic factors by supplying FAs to cancer cells in regions where the glucose demand was insufficient [77]. Additionally, it has been shown that LD production mediated by lysophosphatidylcholine acyltransferase2 increased the resistance of CRC cells to 5-fluorouracil and oxaliplatin [78].

### 3. Discussion

All facts mentioned above justify the additional studies on the metabolism of FAs at the subcellular level.

When analyzing the pathways of the metabolism of FAs in the human colon, one has to remember that FAs gain entrance into the intestine through enterocytes, which are placed on the inner surface of the colon. FAs and monoglycerides (MGs) are able to cross the apical membrane of the intestinal absorptive cells via passive diffusion or high-specialized fatty acid transport protein 4 (FATP4), or CD36 may be involved in this process. Subsequently, FA molecules are bound to intestinal fatty-acid-binding proteins (I-FABP), which transport them to the ER. Scheme 1 shows the simplified pathways of dietary lipid metabolism in human colon cells.



**Scheme 1.** Schematic representation of FA synthesis and metabolism in human colon cells. Explanation of the abbreviations from scheme: **DG**: diacylglycerol, **FA**: fatty acid, **LPA**: lysophosphatidic acid, **MAG**: monoacylglycerol, **TG**: triacylglycerol, **ACC**: acetyl-CoA carboxylase, **ACS**: acetyl-CoA synthetase, **FASN**: fatty acid synthase, **FA-CoA**: fatty acid-coenzyme A, **MAGL**: monoacylglycerol lipase, **MCD**: malonyl-CoA decarboxylase, **CPT1**: carnitine palmitoyltransferase I, **PA**: phosphatidic acid, **PLs**: polar lipids.

The ER is a major hub for the metabolism of FAs, being implicated in uptake of exogenous FAs, de novo synthesis, elongation, and desaturation. The ER is in contact with many other organelles, such as mitochondria, the nucleus, LDs, and peroxisome, via their membranes, which allows efficient transfer of FA substrates and enzymes. The excess FAs present in the ER are used by cells for triacylglycerol (TAG) and cholesterol ester (ChE) synthesis. Subsequently, TAGs and ChEs are stored in LDs or exported through the organism by lipoproteins (many FAs act as specific platforms with high protein affinity and are used as a substrate for protein acylation, affecting their activity and localization). The primary lipoproteins synthesized at the ER in enterocytes are the chylomicrons (CM), also known as ultra-low-density lipoproteins (U LDLs). U LDLs enable fats to move within the water-based solution of the bloodstream (ApoB48 is a protein specific to CM).

Figures 3, 4 and S3–S5 present the analysis of cells using Raman spectroscopy and the analysis of areas corresponding to lipid-rich regions, mitochondria, the nucleus, and the cell membrane. Based on the obtained spectra and Raman images, a spectral analysis of characteristic bands was performed, and in further considerations, based on the identified bands, we analyzed the cellular metabolism of fatty acids, as shown in the Figures 5–10 using the Raman band intensity ratios.

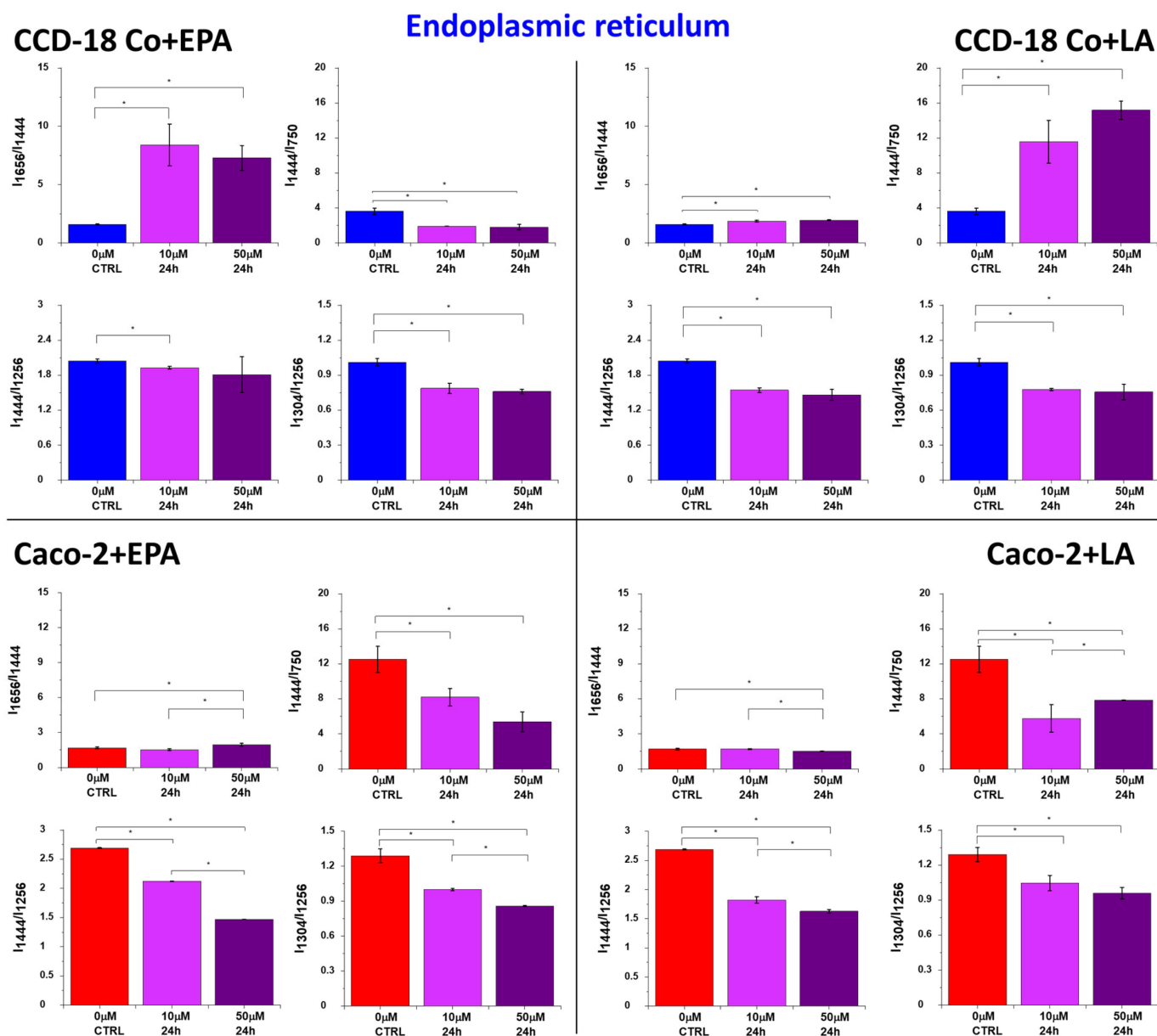


**Figure 5.** Raman band intensities ratios based on peaks typical for lipids (1304, 1444  $\text{cm}^{-1}$ ), proteins/nucleic acids (750  $\text{cm}^{-1}$ ), and proteins (1256, 1656  $\text{cm}^{-1}$ ) calculated based on the mean Raman spectra obtained for the ER (blue cluster in RI data). Data are presented as mean  $\pm$  SD. The statistically significant results, based on ANOVA analysis, have been marked with asterisks (confidence level = 0.05).

The increased number of lipoproteins synthesized at the ER upon FA supplementation can be observed by using Raman spectra. Figure 5 shows the ratios of Raman band intensity characteristic for proteins/nucleic acids (750  $\text{cm}^{-1}$ ), proteins (1256, 1656  $\text{cm}^{-1}$ ), and lipids (1304, 1444  $\text{cm}^{-1}$ ) upon LA and EPA supplementation. The increasing synthesis of proteins specialized in FA transport after the addition of acids, for the ER, is confirmed by the tendency observed for  $I_{1656}/I_{1444}$ ,  $I_{1444}/I_{1256}$ ,  $I_{1304}/I_{1256}$ , and  $I_{1444}/I_{750}$  ratios (decreasing for  $I_{1656}/I_{1444}$  and  $I_{1444}/I_{750}$  and increasing for  $I_{1444}/I_{1256}$  and  $I_{1304}/I_{1256}$ ).

Moreover, the concentration effect is observed, and all regularities are noticed for both types of human colon cells: normal CCD-18 Co and cancer Caco-2.

Lipoproteins synthesized in the ER are then moved to LDs, which are specialized in lipid storage. LDs consist of the core built by neutral lipids, mainly TGAs, ChEs, and a monolayer mainly formed by phospholipids (phosphatidylcholine, phosphatidylethanolamine, and phosphatidylinositol [79]). The surface of LDs is decorated by proteins that are specialized in lipid

metabolism regulation. The first and best-characterized coat protein family is the perilipin protein family, consisting of five proteins: perilipin 1 (PLIN1), perilipin 2 (PLIN2/ADRP), perilipin 3 (PLIN3/TIP47), perilipin 4 (PLIN4/S3-12), and perilipin 5 (PLIN5/OXPAT/LSDP5/MLDP) [80–82]. Figure 6 shows the ratios of Raman band intensities characteristic for proteins/nucleic acids ( $750\text{ cm}^{-1}$ ), proteins (1256,  $1656\text{ cm}^{-1}$ ), and lipids ( $1304$ ,  $1444\text{ cm}^{-1}$ ) in LDs.

The tendency observed for Raman peak intensity ratios in Figure 6 is the expected result for cells faced with the task of intensive transfer of excess FAs to LDs. Moreover, the concentration effect is observed, and all regularities are noticed for both types of human colon cells: normal CCD-18 Co and cancer Caco-2, even if for normal cells the stronger effect is noticed.

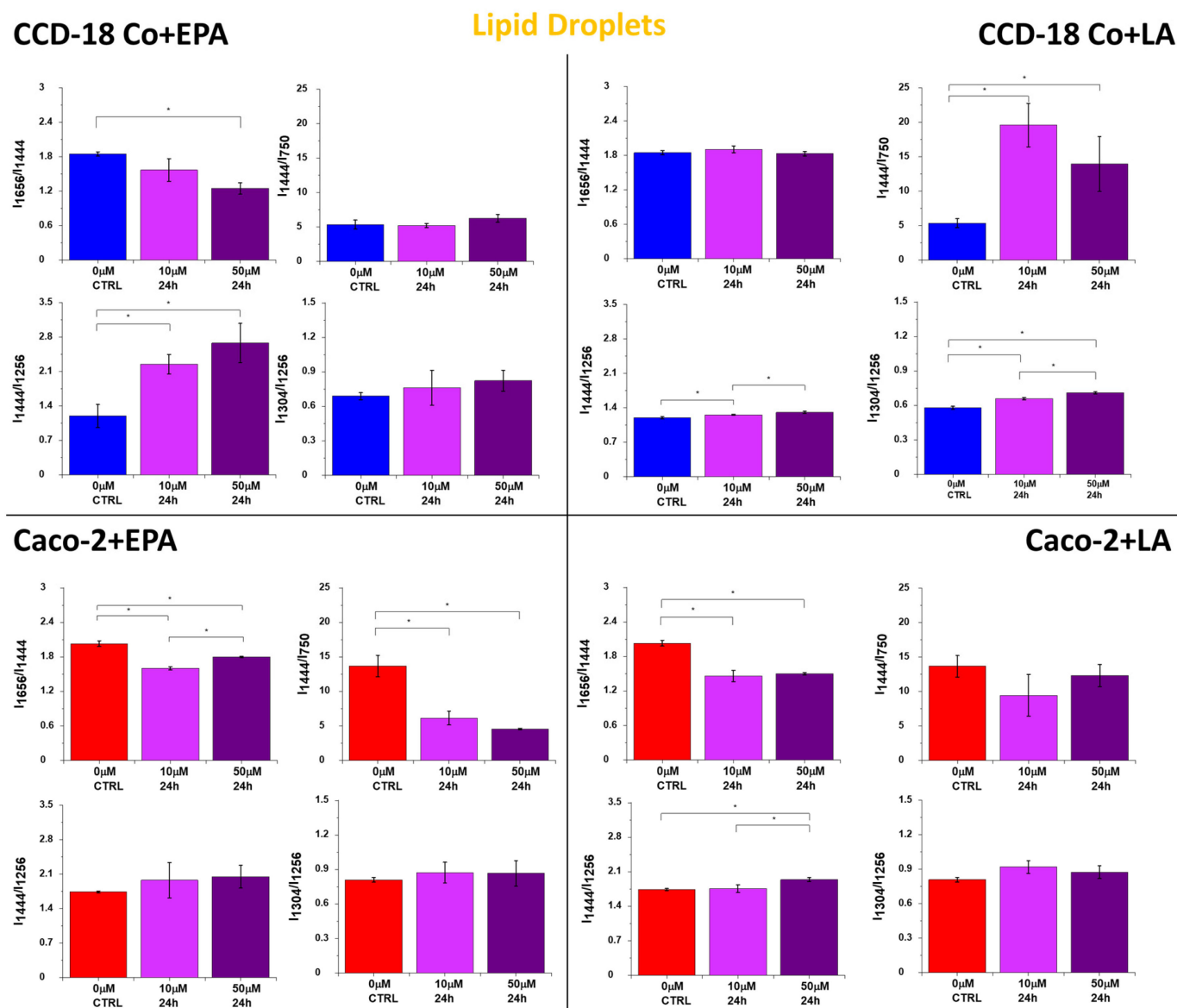


**Figure 6.** Raman band intensity ratios based on peaks typical for lipids ( $1304$ ,  $1444\text{ cm}^{-1}$ ), proteins/nucleic acids ( $750\text{ cm}^{-1}$ ), and proteins ( $1256$ ,  $1656\text{ cm}^{-1}$ ) calculated based on the mean Raman spectra obtained for LDs (orange cluster in RI data). Data are presented as mean  $\pm$  SD. The statistically significant results, based on ANOVA analysis, have been marked with asterisks (confidence level = 0.05).

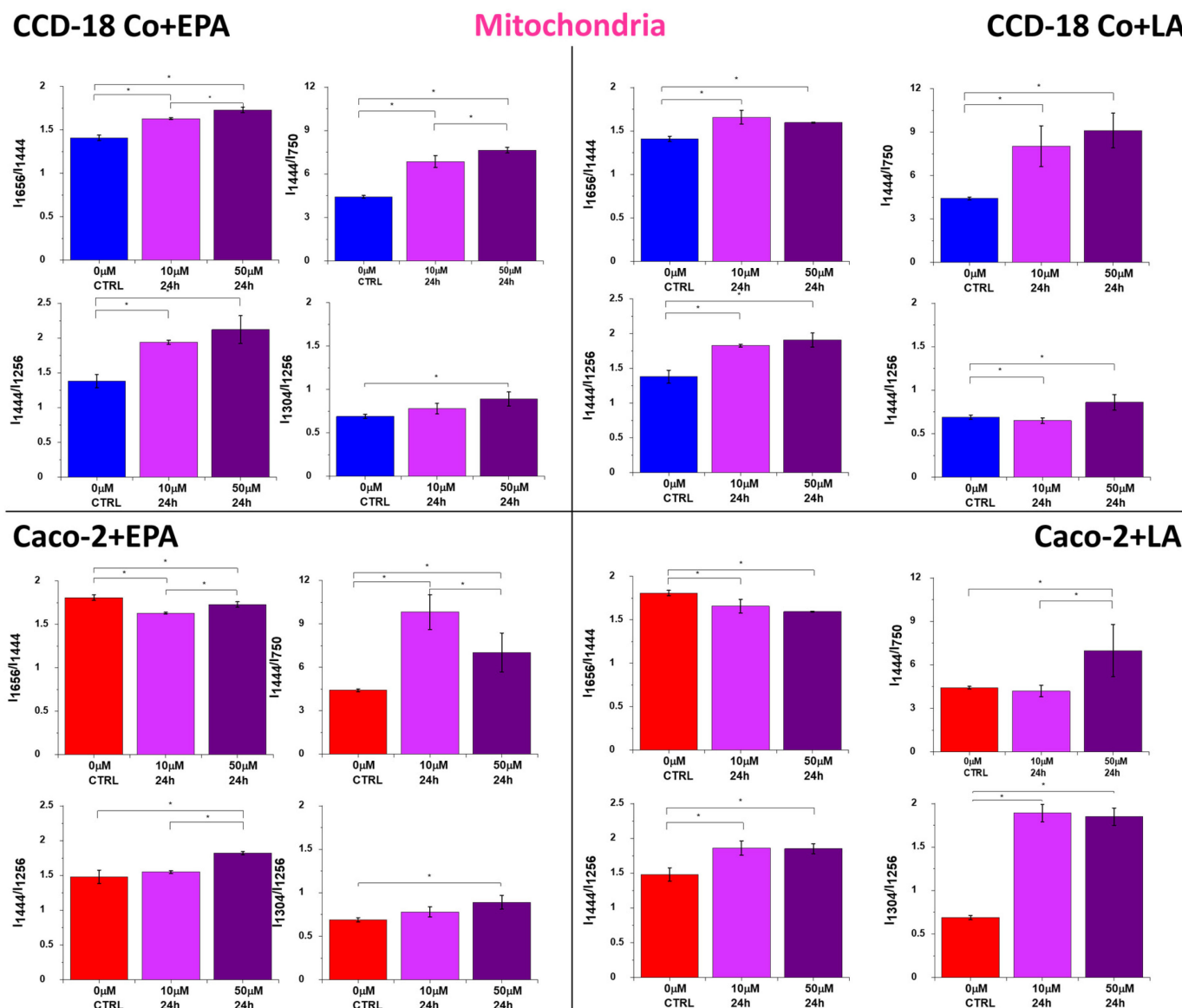


**Figure 7.** Raman band intensity ratios based on peaks typical for lipids (1304, 1444  $\text{cm}^{-1}$ ), nucleic acids (750  $\text{cm}^{-1}$ ), and proteins (1256, 1656  $\text{cm}^{-1}$ ) calculated based on the mean Raman spectra obtained for mitochondria (magenta cluster in RI data). Data are presented as mean  $\pm$  SD. The statistically significant results, based on ANOVA analysis, have been marked with asterisks (confidence level = 0.05).

FAs are also used in mitochondria to produce energy. Mitochondria are responsible for energy production in the form of ATP, which is crucial for the proper functioning of cells. In mitochondria, FAs undergo  $\beta$ -oxidation, which generates acetyl-coenzyme-A, flavin adenine dinucleotide ( $\text{FADH}_2$ ), and nicotinamide adenine dinucleotide (NADH). Mitochondria play a crucial role in the  $\beta$ -oxidation of FAs as they are the site of acetyl-CoA production and the citric acid cycle. However, mitochondrial stress can be observed as a consequence of elevated  $\beta$ -oxidation; increased ROS production may result in cell damage or cell death. Moreover, it should be noted that lipid overload of the mitochondria is directly connected to insulin resistance, which is crucial for type 2 diabetes during obesity. One can see from Figure 7 that all ratios combining the intensity of Raman peaks for proteins/nucleic acids (750  $\text{cm}^{-1}$ ), proteins (1256, 1656  $\text{cm}^{-1}$ ), and lipids (1304, 1444  $\text{cm}^{-1}$ ) confirm the increasing activity of mitochondria in cancer Caco-2 cells; for the normal cells, CCD-18 Co, the correlation is opposite, even if the concentration effect is observed in both types of cells.

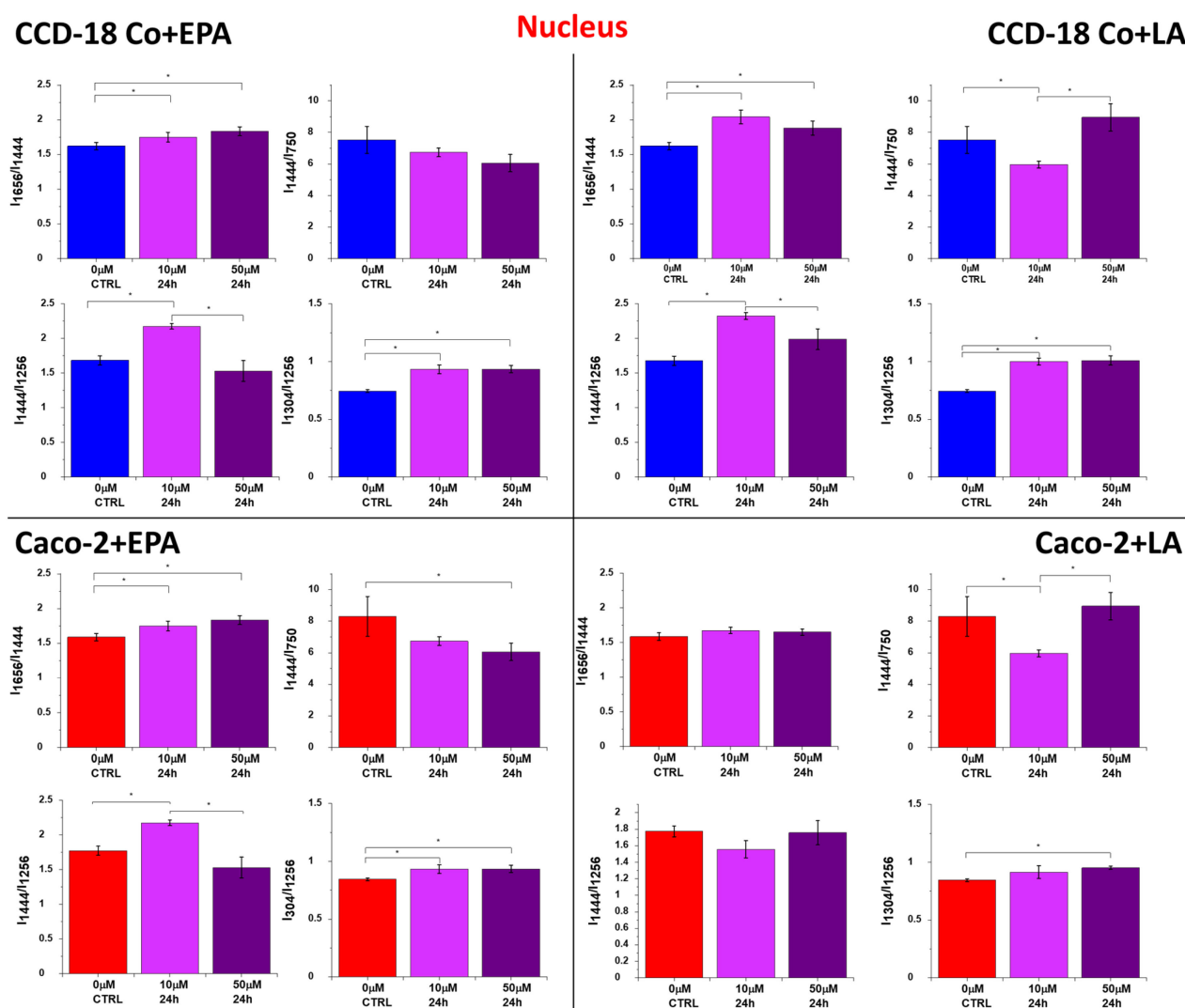


**Figure 8.** Raman band intensity ratios based on peaks typical for lipids (1304, 1444  $\text{cm}^{-1}$ ), nucleic acids (750  $\text{cm}^{-1}$ ), and proteins (1256, 1656  $\text{cm}^{-1}$ ) calculated based on the mean Raman spectra obtained for the nucleus (red cluster in Raman imaging data). Data are presented as means value  $\pm$  SD. The statistically significant results, based on ANOVA analysis, have been marked with asterisks (confidence level = 0.05).

FAs can be also transported to the nucleus. The special role in such a transport is played by the fatty-acid-binding proteins (FABPs), which have the ability to transport FAs not only to the nucleus but also to the mitochondria and ER. FABPs also participate in the uptake of FAs from the extracellular environment. By transporting FAs to the nucleus, FABPs can modulate the activity of nuclear receptors involved in transcriptional regulation. Altered expression of certain FABPs has been observed in various cancers [83]; therefore, FABP levels may serve as cancer development biomarkers. I-FABPs have been investigated as potential biomarkers for IBD [84]. High levels of I-FABPs in serum may indicate intestinal mucosal damage [85]. One can see from Figure 8 that all ratios combining the intensity of Raman peaks for proteins (1256, 1656  $\text{cm}^{-1}$ ), lipids (1304, 1444  $\text{cm}^{-1}$ ), and nucleic acids (750  $\text{cm}^{-1}$ ) confirm the increasing activity of lipoproteins for both types of cells in nucleus. Moreover, the dose effect for EPA and LA is observed.

As we discussed above, the excess consumption of PA, in contrast to UFAs (LA and EPA), can have a negative impact on the human body. To check the correlation between the human colon cell biochemistry and the supplementation type using PUFAs or SFAs,

we have conducted experiments using CCD-18 Co cells and PA. Figure 9 shows the data obtained for CCD-18 Co cells upon the addition of PA.

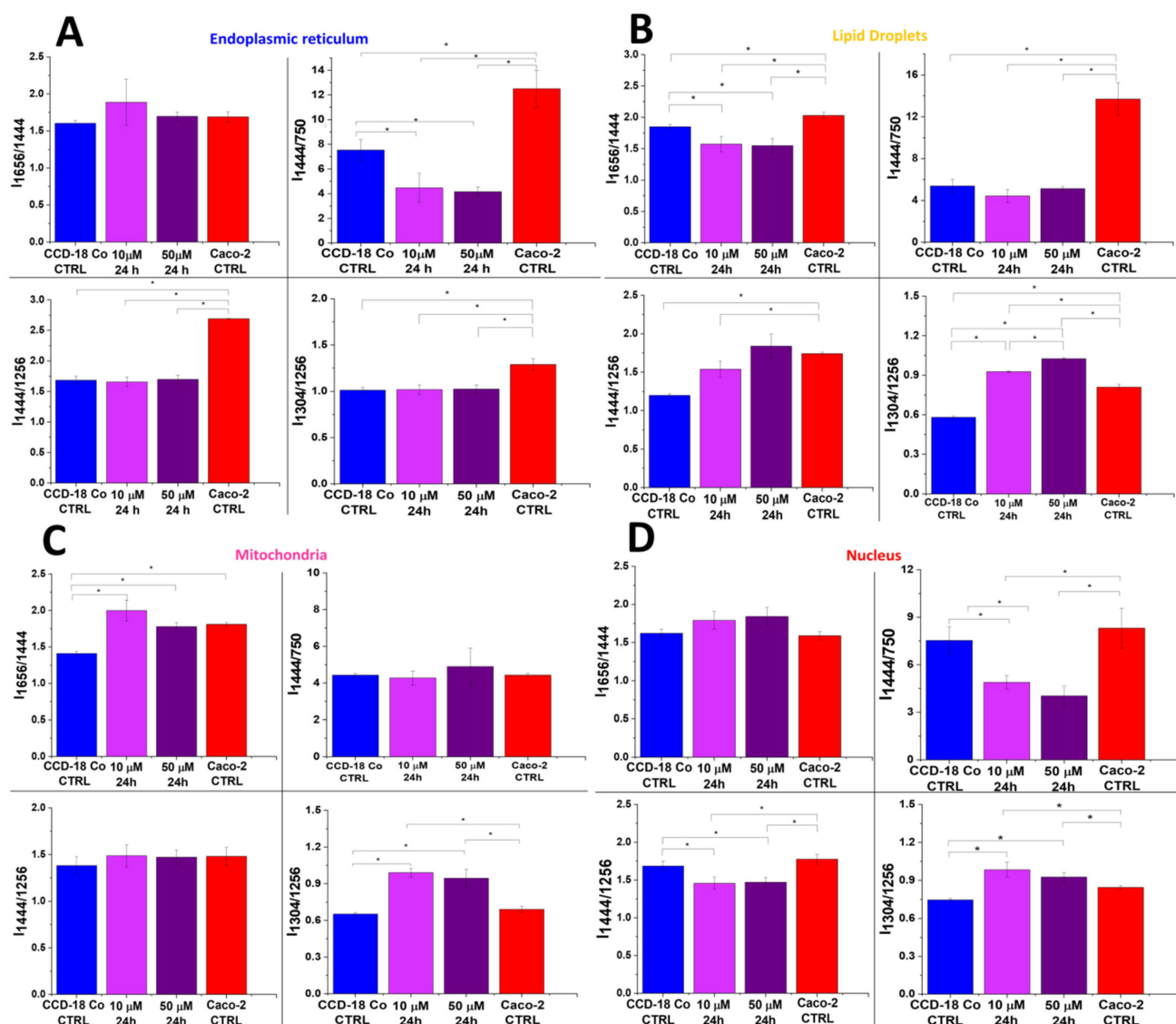


**Figure 9.** Raman band intensity ratios based on peaks typical for lipids ( $1304$ ,  $1444$   $\text{cm}^{-1}$ ), proteins/nucleic acids ( $750$   $\text{cm}^{-1}$ ), and proteins ( $1256$ ,  $1656$   $\text{cm}^{-1}$ ) calculated based on the mean Raman spectra obtained for ER (panel (A), blue cluster in RI data), LDs (panel (B), orange cluster in RI data), mitochondria (panel (C), magenta cluster in RI data), and nucleus (panel (D), red cluster in RI data). Data are presented as means value  $\pm$  SD. The statistically significant results, based on ANOVA analysis, have been marked with asterisks (confidence level = 0.05).

One can see from Figure 9 that after the addition of PA (magenta ( $10$   $\mu\text{M}$ , 24 h) and violet ( $50$   $\mu\text{M}$ , 24 h) bars), Raman band intensity ratios calculated based on peaks typical for lipids ( $1304$ ,  $1444$   $\text{cm}^{-1}$ ) and proteins ( $1256$ ,  $1656$   $\text{cm}^{-1}$ ) for ER, LDs, and mitochondria typical for normal cells become more similar to the ratios typical for cancer cells, excluding dependences observed for the nucleus (which confirm the stability of the chemical composition of this organelle). This observation correlates well with the thesis of the adverse impact of PFAs on human cells.

Because the properties of human cells, membranes depend on the UFA/SFA ratio; Raman data analysis has also been performed for this organelle. Figure 10 presents the results of the studies.

Firstly, one can see from Figure 10 that FAs are effectively built into the cell membranes and, secondly, the strongest effect can be observed for LA.

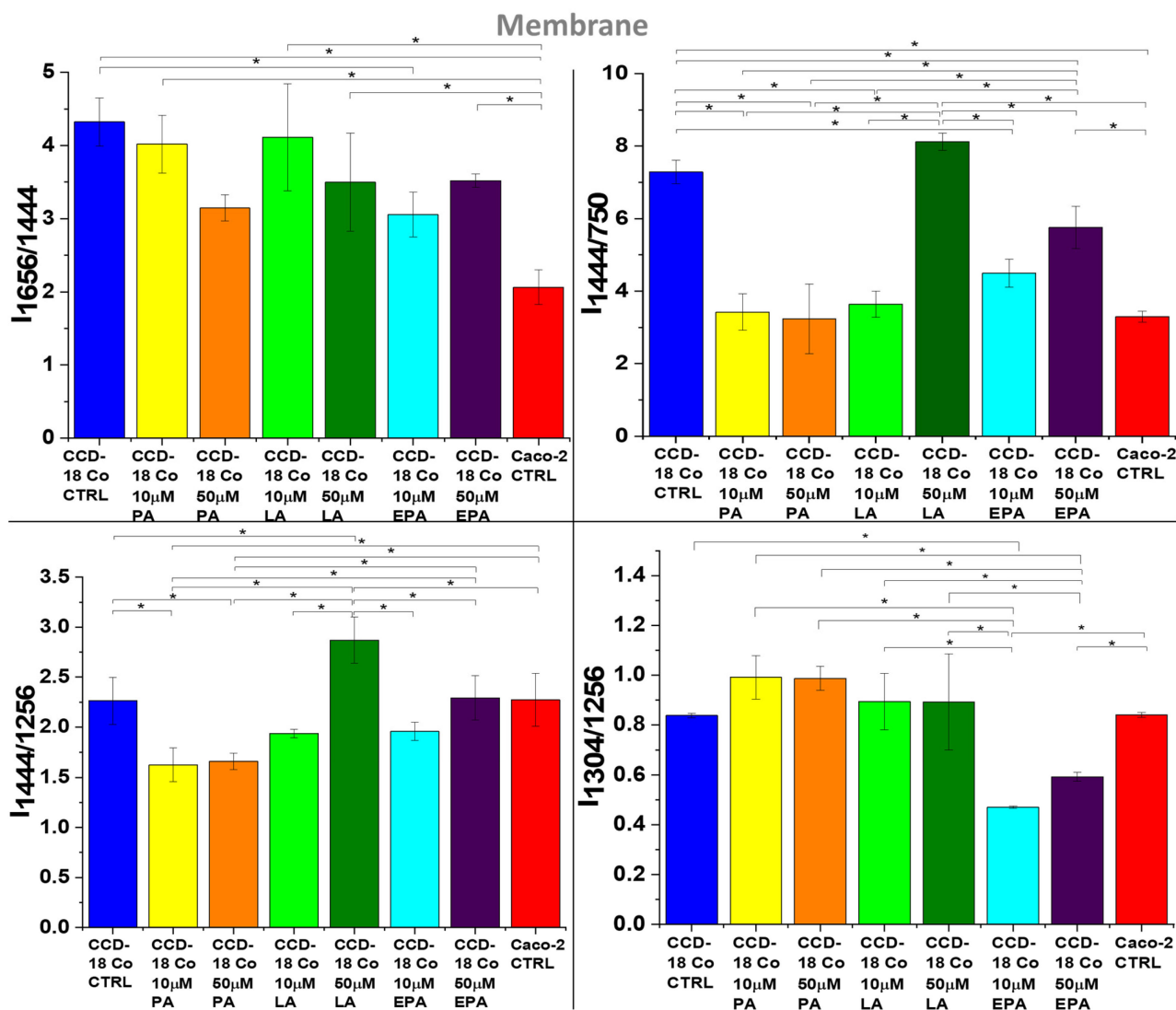


**Figure 10.** Raman band intensity ratios based on peaks typical for lipids (1304, 1444  $\text{cm}^{-1}$ ), proteins/nucleic acids (750  $\text{cm}^{-1}$ ), and proteins (1256, 1656  $\text{cm}^{-1}$ ) calculated based on the mean Raman spectra obtained for membrane (gray cluster in RI data) for normal colon cells—CCD-18 Co (blue), CCD-18 Co upon PA supplementation (10  $\mu\text{M}$ —yellow, 50  $\mu\text{M}$ —orange), CCD-18 Co upon LA supplementation (10  $\mu\text{M}$ —lime, 50  $\mu\text{M}$ —green), CCD-18 Co upon EPA supplementation (10  $\mu\text{M}$ —turquoise, 50  $\mu\text{M}$ —violet), and cancer colon cells—Caco-2 (red). Data are presented as means value  $\pm$  SD. The statistically significant results, based on ANOVA analysis, have been marked with asterisks (confidence level = 0.05).

To confirm the effect of the FA dose and FA type on vibrational properties of human colon cells, we performed a statistical analysis of the data and calculated the Pearson correlation coefficients for all analyzed samples. The Pearson coefficient represents the ratio between the covariance of two variables and their standard deviations and is essentially a normalized measurement of the covariance. Table 1 shows the results of the statistical analysis performed.

**Table 1.** Pearson correlation coefficients calculated based on mean Raman spectra typical for normal human colon cells (CCD-18 Co) and cancer human colon cells (Caco-2) and cells upon FA supplementation. Data for EPA supplementation for 10  $\mu$ M, 24 h, and 50  $\mu$ M, 24 h; LA supplementation for 10  $\mu$ M, 24 h, and 50  $\mu$ M, 24 h; and PA supplementation for 10  $\mu$ M, 24 h, and 50  $\mu$ M, 24 h.

<i>Mean Raman spectrum of</i>	<i>Pearson Correlation Coefficient</i>	<i>p-Value</i>
<i>CCD-18 Co cells</i>		
CCD-18 Co + EPA 10 $\mu$ M, 24 h	0.98592	<0.05
CCD-18 Co + EPA 50 $\mu$ M, 24 h	0.98073	<0.05
CCD-18 Co + LA 10 $\mu$ M, 24 h	0.97283	<0.05
CCD-18 Co + LA 50 $\mu$ M, 24 h	0.97381	<0.05
CCD-18 Co + PA 10 $\mu$ M, 24 h	0.98524	<0.05
CCD-18 Co + PA 50 $\mu$ M, 24 h	0.98133	<0.05
<i>Caco-2 cells</i>		
Caco-2 + EPA 10 $\mu$ M, 24 h	0.99138	<0.05
Caco-2 + EPA 50 $\mu$ M, 24 h	0.95889	<0.05
Caco-2 + LA 10 $\mu$ M, 24 h	0.96872	<0.05
Caco-2 + LA 50 $\mu$ M, 24 h	0.96572	<0.05
CCD-18 Co + PA 10 $\mu$ M, 24 h	0.96862	<0.05
CCD-18 Co + PA 50 $\mu$ M, 24 h	0.98119	<0.05

## 4. Materials and Methods

### 4.1. Cell Lines and Cell Culture

The CCD-18 Co cell line (ATCC<sup>®</sup> CRL-1459<sup>™</sup>) was purchased from ATCC: The Global Bioresource Center (10801 University Blvd. Manassas, VA 20110, USA). The CCD-18 Co cell line was cultured using ATCC-formulated Eagle's Minimum Essential Medium with L-glutamine (catalog No. 30-2003). To make the complete growth medium, fetal bovine serum was added to a final concentration of 10%. Every 2–3 days, a new medium was used. The cells obtained from the patient were normal myofibroblasts in the colon. The biological safety of the CCD-18 Co cell line has been classified by the American Biosafety Association (ABSA) as level 1 (BSL-1). The Caco-2 cell line was also purchased from ATCC and cultured according to the ATCC protocols. The Caco-2 cell line was obtained from a patient—a 72-year-old Caucasian male diagnosed with colon adenocarcinoma. The biological safety of the obtained material is classified as level 1 (BSL-1). To complete the medium, it was based on Eagle's Minimum Essential Medium with L-glutamine, with the addition of fetal bovine serum to a final concentration of 20%. The medium was renewed once or twice a week.

### 4.2. Cultivation Conditions

The cell lines (CCD-18 Co and Caco-2) used in the experiments in this study were grown in flat-bottom culture flasks made of polystyrene with a cell growth surface of 75 cm<sup>2</sup>. Flasks containing cells were stored in an incubator providing the following environmental conditions: 37 °C, 5% CO<sub>2</sub>, and 95% air.

Cells used for research were seeded onto CaF<sub>2</sub> windows (25 × 1 mm) at a low density of 10<sup>4</sup> cells/cm<sup>2</sup>. After 24 h incubation on the CaF<sub>2</sub>, the standard growth medium was removed, and fatty acid solution diluted in medium in concentrations 10  $\mu$ M and 50  $\mu$ M was added for 24 h. After this time, the cells were rinsed with PBS (phosphate-buffered saline, Gibco, 10010023, pH 7.4 at 25 °C, 0.01 M) and then cells were fixed with formaldehyde (4% buffered formalin) for 10 min and washed once more with PBS. The Raman confocal measurements were made immediately after the fixation of the samples. All the fatty acid

solutions used for the supplementation procedure in the investigation were prepared by diluting the compound in the pure culture medium.

#### 4.3. Raman Imaging

All maps and Raman spectra presented and discussed in this paper were recorded using the confocal microscope Alpha 300 RSA+ (WITec, Ulm, Germany) equipped with an Olympus microscope integrated with an ultra-high-throughput spectrometer and a CCD camera. The average excitation power of the 532 nm excitation laser during the experiments was 10 mW (measured after the beam passed through the objective), with an integration time of 0.5 s for the low-frequency region. The laser was focused on the sample through a Nikon objective lens with magnification of 40 $\times$ , intended for cell measurements performed via immersion in PBS. Spectral images were collected with a sampling density of 0.5  $\mu\text{m}$  (the z-axis step size was equal to 1.5  $\mu\text{m}$ ). The obtained Raman spectra and all imaging data were analyzed using cluster analysis (CA), which was executed using the WITec Project Plus package (for the removal of cosmic rays and smoothing and background corrections). More details about the equipment, settings, and parameters can be found in previous works [66,67,86–88].

The normalization model, divided by norm (divide the spectrum by the dataset norm), was performed using Origin 2021 software according to the following formula:

$$V' = \frac{V}{\|V\|}$$
$$\|V\| = \sqrt{v_1^2 + v_2^2 + \dots + v_n^2}$$

where  $v_n$  is the  $n^{\text{th}}$   $V$  value.

The normalization was performed for all Raman spectra presented in the manuscript. Origin software was also used to perform the ANOVA analysis, which was necessary to indicate statistically significant results (means comparison: Tukey model; significance level: 0.05).

#### 4.4. Determination of the Appropriate Concentration of FAs Using the XTT Test

For each cell type, XTT ((2,3-Bis-(2-Methoxy-4-Nitro-5-Sulfophenyl)-2H-Tetrazolium-5-Carboxanilide) proliferation kit, catalogue number 20-300-1000, Biological Industries) tests were performed 24 h after the addition of FAs to the cells immersed in the culture medium. Preparation for the test included proper filling of the 96-well plate according to the procedure developed at the Institute of Applied Radiation Chemistry in Lodz. The wells were filled in such a way that each row contained a specific series of measurements. For example, in one row, all plates were filled with the medium; in another, the plates were filled with control samples containing only cells immersed in the medium; and in subsequent rows, plates were filled with cells in the medium with the addition of a specific concentration of FAs. Different concentrations of FAs were selected for the test:

1. For PA: 1  $\mu\text{M}$ , 5  $\mu\text{M}$ , 10  $\mu\text{M}$ , 25  $\mu\text{M}$ , 50  $\mu\text{M}$ , and 100  $\mu\text{M}$ .
2. For LA and EPA: 1  $\mu\text{M}$ , 5  $\mu\text{M}$ , 10  $\mu\text{M}$ , 25  $\mu\text{M}$ , 50  $\mu\text{M}$ , and 100  $\mu\text{M}$ .

After filling all of the 96-well plates, the samples were incubated at 37  $^{\circ}\text{C}$ . After 24 h from the addition of FAs, the XTT test was performed using Varioscan LUX Multimode Plate Reader from Thermo Fisher Scientific (Waltham, MA, USA). The measurement took about 3 h. After the completion of the study, the obtained results were analyzed using a spreadsheet, resulting in a bar graph showing the effect of the concentration of FAs on the survival of the tested cell type, taking into account the time since the addition of FAs.

Figure S2 shows the XTT viability tests conducted on human normal colon cells and human colon cancer cells supplemented with LA (Linoleic Acid, L1376, Merck Life Science Sp. z o. o, Warsaw, Poland), EPA (*cis*-5,8,11,14,17-eicosapentaenoic Acid, E2011, Merck Life Science Sp. z o. o, Warsaw, Poland), and PA (Palmitic Acid, (P0500), Merck Life Science Sp.

z o. o, Warsaw, Poland). Please see Supplementary Materials for XTT viability test dates and a detailed description of the obtained results.

## 5. Conclusions

Using Raman imaging, we have proved that mapping mode can be effectively used to visualize single-cell substructures, which is helpful in the analysis of FA metabolic pathways. Using the cluster analysis algorithm, we have visualized the endoplasmic reticulum (ER), mitochondria, lipid droplets (LDs), and nucleus—the major organelles involved in the metabolism of FAs. We have analyzed the chemical composition of these organelles without and upon FA supplementation. Analysis of Raman band intensity ratios typical for lipids, proteins, and nucleic acids ( $I_{1656}/I_{1444}$ ,  $I_{1444}/I_{1256}$ ,  $I_{1444}/I_{750}$ , and  $I_{1304}/I_{1256}$ ) proved that using Raman mapping, we can observe the metabolic pathways of FAs in various cellular compartments, including in ER, which is responsible for the uptake of exogenous FAs, de novo synthesis, elongation, and desaturation; in mitochondria, responsible for energy production; in LDs, specialized in fat storage; and in the nucleus, where fatty acids are transported via fatty-acid-binding proteins. These pathways serve as biomarkers of human colon cancerogenesis. Moreover, Raman studies of cell membrane composition showed the effective incorporation of FA molecules, with the strongest effect for LA. The spectroscopy studies were completed with XTT tests, which showed that the addition of LA or EPA for Caco-2 cells decreases their viability with a stronger effect observed for LA; the opposite effect was observed for PA. For normal cells, CCD-18 Co supplementation using LA or EPA stimulated cell growth, while PA had the opposite effect.

**Supplementary Materials:** The following supporting information can be downloaded at: <https://www.mdpi.com/article/10.3390/ijms25084508/s1>.

**Author Contributions:** Conceptualization: B.B.-P.; funding acquisition: K.B.-M.; investigation: K.B.-M., M.K. and B.B.-P.; methodology: K.B.-M., B.B.-P. and M.K.; writing—original draft: K.B.-M. and B.B.-P.; manuscript editing: K.B.-M., B.B.-P. and M.K. All authors reviewed and provided feedback on the manuscripts. All authors have read and agreed to the published version of the manuscript.

**Funding:** This research was funded by grant No. W3/6D/2022 from the FU<sup>2</sup>N—Young Scientists' Skills Improvement Fund at the Lodz University of Technology "Biochemical and nanomechanical analysis of human digestive system cells using atomic force microscopy and Raman spectroscopy and imaging. Effect of fatty acid supplementation on cell biochemistry and morphology". The funders had no role in the design of the study; in the collection, analyses, or interpretation of data; in the writing of the manuscript; or in the decision to publish the results.

**Institutional Review Board Statement:** Not applicable.

**Informed Consent Statement:** Not applicable.

**Data Availability Statement:** The raw data underlying the results presented in the study are available on request. Requests for access to those data should be addressed to the Head of Laboratory of Laser Molecular Spectroscopy, Institute of Applied Radiation Chemistry, Lodz University of Technology. Data requests may be sent by email to the Secretary of the Institute of Applied Radiation Chemistry: w3i34@adm.p.lodz.pl.

**Acknowledgments:** This article was completed while the first author was a Doctoral Candidate in the Interdisciplinary Doctoral School at Lodz University of Technology, Poland.

**Conflicts of Interest:** The authors declare no conflict of interest. The funders had no role in the design of the study; in the collection, analyses, or interpretation of data; in the writing of the manuscript, or in the decision to publish the results.

## References

1. Pakiet, A.; Kobiela, J.; Stepnowski, P.; Sledzinski, T.; Mika, A. Changes in lipids composition and metabolism in colorectal cancer: A review. *Lipids Health Dis.* **2019**, *18*, 29. [[CrossRef](#)] [[PubMed](#)]
2. Fernández, L.P.; Gómez de Cedrón, M.; Ramírez de Molina, A. Alterations of Lipid Metabolism in Cancer: Implications in Prognosis and Treatment. *Front. Oncol.* **2020**, *10*, 577420. [[CrossRef](#)] [[PubMed](#)]

3. Hamilton, S.D.; Vogelstein, B.; Kudo, S.; Riboli, E.; Nakamura, S.H.; Hainaut, P.; Rubio, C.A.; Sobin, L.H.; Fogt, F.; Winawer, S.J.; et al. Tumours of the colon and rectum: Carcinoma of the colon and rectum. In *World Health Organization Classification of Tumours: Pathology and Genetics of Tumours of the Digestive System*; Hamilton, S.R., Aaltonen, L.A., Eds.; IARC Press: Lyon, France, 2000; pp. 105–119. ISBN 92 832 24108.
4. Laredo, V.; García-Mateo, S.; Martínez-Domínguez, S.J.; López de la Cruz, J.; Gargallo-Puyuelo, C.J.; Gomollón, F. Risk of Cancer in Patients with Inflammatory Bowel Diseases and Keys for Patient Management. *Cancers* **2023**, *15*, 871. [[CrossRef](#)] [[PubMed](#)]
5. Liu, X.; Jakubowski, M.; Hunt, J.L. KRAS Gene Mutation in Colorectal Cancer Is Correlated with Increased Proliferation and Spontaneous Apoptosis. *Am. J. Clin. Pathol.* **2011**, *135*, 245–252. [[CrossRef](#)] [[PubMed](#)]
6. Georgescu, C.V.; Săftoiu, A.; Georgescu, C.C.; Ciurea, R.; Ciurea, T. Correlations of proliferation markers, p53 expression and histological findings in colorectal carcinoma. *J. Gastrointest. Liver Dis.* **2007**, *16*, 133–139. [[PubMed](#)]
7. Koppenol, W.H.; Bounds, P.L.; Dang, C.V. Otto Warburg's contributions to current concepts of cancer metabolism. *Nat. Rev. Cancer* **2011**, *11*, 325–337. [[CrossRef](#)]
8. Xu, X.D.; Shao, S.X.; Jiang, H.P.; Cao, Y.W.; Wang, Y.H.; Yang, X.C.; Wang, Y.L.; Wang, X.S.; Niu, H.T. Warburg Effect or Reverse Warburg Effect? A Review of Cancer Metabolism. *Oncol. Res. Treat.* **2015**, *38*, 117–122. [[CrossRef](#)] [[PubMed](#)]
9. LIPID MAPS®. Lipidomics Gateway. Available online: [https://www.lipidmaps.org/data/classification/lipid\\_cns.html](https://www.lipidmaps.org/data/classification/lipid_cns.html) (accessed on 13 February 2024).
10. Fahy, E.; Cotter, D.; Sud, M.; Subramaniam, S. Lipid classification, structures and tools. *Biochim. Biophys. Acta Mol. Cell Biol. Lipids* **2011**, *1811*, 637–647. [[CrossRef](#)] [[PubMed](#)]
11. Goodhart, R.S.; Shils, M.E.; Maurice, E.; Goodhart, R.S. *Modern Nutrition in Health and Disease*, 6th ed.; Lea & Febiger: Philadelphia, PA, USA, 1980; ISBN 0812106458.
12. Hidalgo, M.A.; Carretta, M.D.; Burgos, R.A. Long Chain Fatty Acids as Modulators of Immune Cells Function: Contribution of FFA1 and FFA4 Receptors. *Front. Physiol.* **2021**, *12*, 668330. [[CrossRef](#)] [[PubMed](#)]
13. Mthembu, S.X.H.; Mazibuko-Mbeje, S.E.; Silvestri, S.; Orlando, P.; Marcheggiani, F.; Cirilli, I.; Nkambule, B.B.; Muller, C.J.F.; Tiano, L.; Dłudla, P.V. Low levels and partial exposure to palmitic acid improves mitochondrial function and the oxidative status of cultured cardiomyoblasts. *Toxicol. Rep.* **2024**, *12*, 234–243. [[CrossRef](#)] [[PubMed](#)]
14. Carta, G.; Murru, E.; Banni, S.; Manca, C. Palmitic Acid: Physiological Role, Metabolism and Nutritional Implications. *Front. Physiol.* **2017**, *8*, 902. [[CrossRef](#)]
15. Murru, E.; Manca, C.; Carta, G.; Banni, S. Impact of Dietary Palmitic Acid on Lipid Metabolism. *Front. Nutr.* **2022**, *9*, 861664. [[CrossRef](#)] [[PubMed](#)]
16. French, M.A.; Sundram, K.; Clandinin, M.T. Cholesterolaemic effect of palmitic acid in relation to other dietary fatty acids. *Asia Pac. J. Clin. Nutr.* **2002**, *11* (Suppl. 7), S401–S407. [[CrossRef](#)] [[PubMed](#)]
17. Annevelink, C.E.; Sapp, P.A.; Petersen, K.S.; Shearer, G.C.; Kris-Etherton, P.M. Diet-derived and diet-related endogenously produced palmitic acid: Effects on metabolic regulation and cardiovascular disease risk. *J. Clin. Lipidol.* **2023**, *17*, 577–586. [[CrossRef](#)] [[PubMed](#)]
18. Zock, P.L.; De Vries, J.H.M.; Katan, M.B.; Katan, M.B. Impact of Myristic Acid Versus Palmitic Acid on Serum Lipid and Lipoprotein Levels in Healthy Women and Men. *Arterioscler. Thromb.* **1994**, *14*, 567–575. [[CrossRef](#)] [[PubMed](#)]
19. Nestel, P.; Clifton, P.; Noakes, M. Effects of increasing dietary palmitoleic acid compared with palmitic and oleic acids on plasma lipids of hypercholesterolemic men. *J. Lipid Res.* **1994**, *35*, 656–662. [[CrossRef](#)] [[PubMed](#)]
20. Shao, T.; Verma, H.K.; Pande, B.; Costanzo, V.; Ye, W.; Cai, Y.; Bhaskar, L.V.K.S. Physical Activity and Nutritional Influence on Immune Function: An Important Strategy to Improve Immunity and Health Status. *Front. Physiol.* **2021**, *12*, 751374. [[CrossRef](#)] [[PubMed](#)]
21. Dang, Y.; Ma, C.; Chen, K.; Chen, Y.; Jiang, M.; Hu, K.; Li, L.; Zeng, Z.; Zhang, H. The Effects of a High-Fat Diet on Inflammatory Bowel Disease. *Biomolecules* **2023**, *13*, 905. [[CrossRef](#)] [[PubMed](#)]
22. Tanaka, S.; Nemoto, Y.; Takei, Y.; Morikawa, R.; Oshima, S.; Nagaiishi, T.; Okamoto, R.; Tsuchiya, K.; Nakamura, T.; Stutte, S.; et al. High-fat diet-derived free fatty acids impair the intestinal immune system and increase sensitivity to intestinal epithelial damage. *Biochem. Biophys. Res. Commun.* **2020**, *522*, 971–977. [[CrossRef](#)] [[PubMed](#)]
23. Wang, X.; Zhang, C.; Bao, N. Molecular mechanism of palmitic acid and its derivatives in tumor progression. *Front. Oncol.* **2023**, *13*, 1224125. [[CrossRef](#)] [[PubMed](#)]
24. Lin, L.; Ding, Y.; Wang, Y.; Wang, Z.; Yin, X.; Yan, G.; Zhang, L.; Yang, P.; Shen, H. Functional lipidomics: Palmitic acid impairs hepatocellular carcinoma development by modulating membrane fluidity and glucose metabolism. *Hepatology* **2017**, *66*, 432–448. [[CrossRef](#)] [[PubMed](#)]
25. Sun, Q.; Yu, X.; Peng, C.; Liu, N.; Chen, W.; Xu, H.; Wei, H.; Fang, K.; Dong, Z.; Fu, C.; et al. Activation of SREBP-1c alters lipogenesis and promotes tumor growth and metastasis in gastric cancer. *Biomed. Pharmacother.* **2020**, *128*, 110274. [[CrossRef](#)] [[PubMed](#)]
26. Zhang, L.; Lv, J.; Chen, C.; Wang, X. Roles of acyl-CoA synthetase long-chain family member 5 and colony stimulating factor 2 in inhibition of palmitic or stearic acids in lung cancer cell proliferation and metabolism. *Cell Biol. Toxicol.* **2021**, *37*, 15–34. [[CrossRef](#)] [[PubMed](#)]
27. Pascual, G.; Domínguez, D.; Benitah, S.A. The contributions of cancer cell metabolism to metastasis. *Dis. Model. Mech.* **2018**, *11*, dmm032920. [[CrossRef](#)] [[PubMed](#)]

28. Gillingham, L.G.; Harris-Janz, S.; Jones, P.J.H. Dietary Monounsaturated Fatty Acids Are Protective Against Metabolic Syndrome and Cardiovascular Disease Risk Factors. *Lipids* **2011**, *46*, 209–228. [[CrossRef](#)] [[PubMed](#)]
29. Lunn, J.; Theobald, H.E. The health effects of dietary unsaturated fatty acids. *Nutr. Bull.* **2006**, *31*, 178–224. [[CrossRef](#)]
30. Watkins, P.A. Fatty acids: Metabolism. *Encycl. Hum. Nutr.* **2013**, *2–4*, 220–230. [[CrossRef](#)]
31. de Souza, C.O.; Teixeira, A.A.S.; Biondo, L.A.; Lima Junior, E.A.; Batatinha, H.A.P.; Rosa Neto, J.C. Palmitoleic Acid Improves Metabolic Functions in Fatty Liver by PPAR $\alpha$ -Dependent AMPK Activation. *J. Cell. Physiol.* **2017**, *232*, 2168–2177. [[CrossRef](#)]
32. Whelan, J.; Fritsche, K. Linoleic acid. *Adv. Nutr.* **2013**, *4*, 311–312. [[CrossRef](#)] [[PubMed](#)]
33. Ziboh, V.A. The importance of linoleic acid metabolites in cancer metastasis and in the synthesis and actions of 13-HODE. *Adv. Exp. Med. Biol.* **1997**, *433*, 291–294. [[CrossRef](#)]
34. den Hartigh, L.J. Conjugated Linoleic Acid Effects on Cancer, Obesity, and Atherosclerosis: A Review of Pre-Clinical and Human Trials with Current Perspectives. *Nutrients* **2019**, *11*, 370. [[CrossRef](#)] [[PubMed](#)]
35. Ha, Y.L.; Grimm, N.K.; Pariza, M.W. Anticarcinogens from fried ground beef: Heat-altered derivatives of linoleic acid. *Carcinogenesis* **1987**, *8*, 1881–1887. [[CrossRef](#)] [[PubMed](#)]
36. Ip, M.M.; Masso-Welch, P.A.; Ip, C. Prevention of mammary cancer with conjugated linoleic acid: Role of the stroma and the epithelium. *J. Mammary Gland. Biol. Neoplasia* **2003**, *8*, 103–118. [[CrossRef](#)] [[PubMed](#)]
37. Liew, C.; Schut, H.A.J.; Chin, S.F.; Pariza, M.W.; Dashwood, R.H. Protection of conjugated linoleic acids against 2-amino-3-methylimidazo[4,5-f]quinoline-induced colon carcinogenesis in the F344 rat: A study of inhibitory mechanisms. *Carcinogenesis* **1995**, *16*, 3037–3043. [[CrossRef](#)] [[PubMed](#)]
38. Ha, Y.L.; Storkson, J.; Pariza, M.W. Inhibition of Benzo(a)pyrene-induced Mouse Forestomach Neoplasia by Conjugated Dienoic Derivatives of Linoleic Acid1. *Cancer Res.* **1990**, *50*, 1097–1101. [[PubMed](#)]
39. Cesano, A.; Visonneau, S.; Scimeca, J.A.; Kritchevsky, D.; Santoli, D. Opposite effects of linoleic acid and conjugated linoleic acid on human prostatic cancer in SCID mice. *Anticancer Res.* **1998**, *18*, 1429–1434. [[PubMed](#)]
40. Lucanic, M.; Held, J.M.; Vantipalli, M.C.; Klang, I.M.; Graham, J.B.; Gibson, B.W.; Lithgow, G.J.; Gill, M.S. N-acyl ethanolamine signalling mediates the effect of diet on lifespan in *Caenorhabditis elegans*. *Nature* **2011**, *473*, 226–229. [[CrossRef](#)] [[PubMed](#)]
41. Bie, N.; Han, L.; Meng, M.; Zhang, Y.; Guo, M.; Wang, C. Anti-tumor mechanism of eicosapentaenoic acid (EPA) on ovarian tumor model by improving the immunomodulatory activity in F344 rats. *J. Funct. Foods* **2020**, *65*, 103739. [[CrossRef](#)]
42. Ando, N.; Hara, M.; Shiga, K.; Yanagita, T.; Takasu, K.; Nakai, N.; Maeda, Y.; Hirokawa, T.; Takahashi, H.; Ishiguro, H.; et al. Eicosapentaenoic acid suppresses angiogenesis via reducing secretion of IL-6 and VEGF from colon cancer-associated fibroblasts. *Oncol. Rep.* **2019**, *42*, 339–349. [[CrossRef](#)] [[PubMed](#)]
43. Olaf, A. Dietary fatty acids and immune reactions in synovial tissue—PubMed. *Eur. J. Med. Res.* **2003**, *8*, 381–387.
44. Pappalardo, G.; Almeida, A.; Ravasco, P. Eicosapentaenoic acid in cancer improves body composition and modulates metabolism. *Nutrition* **2015**, *31*, 549–555. [[CrossRef](#)] [[PubMed](#)]
45. Uematsu, M.; Kita, Y.; Shimizu, T.; Shindou, H. Multiplex fatty acid imaging inside cells by Raman microscopy. *FASEB J.* **2020**, *34*, 10357–10372. [[CrossRef](#)] [[PubMed](#)]
46. Uematsu, M.; Shimizu, T. Raman microscopy-based quantification of the physical properties of intracellular lipids. *Commun. Biol.* **2021**, *4*, 1176. [[CrossRef](#)] [[PubMed](#)]
47. Paramitha, P.N.; Zakaria, R.; Maryani, A.; Kusaka, Y.; Andriana, B.B.; Hashimoto, K.; Nakazawa, H.; Kato, S.; Sato, H. Raman study on lipid droplets in hepatic cells co-cultured with fatty acids. *Int. J. Mol. Sci.* **2021**, *22*, 7378. [[CrossRef](#)] [[PubMed](#)]
48. Toledo, D.A.M.; Roque, N.R.; Teixeira, L.; Milán-Garcés, E.A.; Carneiro, A.B.; Almeida, M.R.; Andrade, G.F.S.; Martins, J.S.; Pinho, R.R.; Freire-de-Lima, C.G.; et al. Lipid Body Organelles within the Parasite *Trypanosoma cruzi*: A Role for Intracellular Arachidonic Acid Metabolism. *PLoS ONE* **2016**, *11*, e0160433. [[CrossRef](#)] [[PubMed](#)]
49. Majzner, K.; Kochan, K.; Kachamakova-Trojanowska, N.; Maslak, E.; Chlopicki, S.; Baranska, M. Raman imaging providing insights into chemical composition of lipid droplets of different size and origin: In hepatocytes and endothelium. *Anal. Chem.* **2014**, *86*, 6666–6674. [[CrossRef](#)]
50. Rensonnet, A.; Tipping, W.J.; Malherbe, C.; Faulds, K.; Eppe, G.; Graham, D. Spectral fingerprinting of cellular lipid droplets using stimulated Raman scattering microscopy and chemometric analysis. *Analyst* **2024**, *149*, 553–562. [[CrossRef](#)] [[PubMed](#)]
51. Czamara, K.; Majzner, K.; Selmi, A.; Baranska, M.; Ozaki, Y.; Kaczor, A. Unsaturated lipid bodies as a hallmark of inflammation studied by Raman 2D and 3D microscopy. *Sci. Rep.* **2017**, *7*, 40889. [[CrossRef](#)] [[PubMed](#)]
52. Fu, D.; Yu, Y.; Folick, A.; Currie, E.; Farese, R.V.; Tsai, T.H.; Xie, X.S.; Wang, M.C. In vivo metabolic fingerprinting of neutral lipids with hyperspectral stimulated raman scattering microscopy. *J. Am. Chem. Soc.* **2014**, *136*, 8820–8828. [[CrossRef](#)]
53. Majzner, K.; Tott, S.; Roussille, L.; Deckert, V.; Chlopicki, S.; Baranska, M. Uptake of fatty acids by a single endothelial cell investigated by Raman spectroscopy supported by AFM. *Analyst* **2018**, *143*, 970–980. [[CrossRef](#)]
54. Park, J.M.; Jeong, M.; Kim, E.H.; Han, Y.M.; Kwon, S.H.; Hahm, K.B. Omega-3 Polyunsaturated Fatty Acids Intake to Regulate *Helicobacter pylori*-Associated Gastric Diseases as Nonantimicrobial Dietary Approach. *Biomed. Res. Int.* **2015**, *2015*, 712363. [[CrossRef](#)]
55. Park, M.; Kim, H. Anti-cancer Mechanism of Docosahexaenoic Acid in Pancreatic Carcinogenesis: A Mini-review. *J. Cancer Prev.* **2017**, *22*, 1. [[CrossRef](#)] [[PubMed](#)]

56. Ding, Y.; Mullapudi, B.; Torres, C.; Mascariñas, E.; Mancinelli, G.; Diaz, A.M.; McKinney, R.; Barron, M.; Schultz, M.; Heiferman, M.; et al. Omega-3 Fatty Acids Prevent Early Pancreatic Carcinogenesis via Repression of the AKT Pathway. *Nutrients* **2018**, *10*, 1289. [[CrossRef](#)] [[PubMed](#)]
57. Calviello, G.; Resci, F.; Serini, S.; Piccioni, E.; Toesca, A.; Boninsegna, A.; Monego, G.; Ranelletti, F.O.; Palozza, P. Docosahexaenoic acid induces proteasome-dependent degradation of beta-catenin, down-regulation of survivin and apoptosis in human colorectal cancer cells not expressing COX-2. *Carcinogenesis* **2007**, *28*, 1202–1209. [[CrossRef](#)] [[PubMed](#)]
58. Stephenson, J.A.; Al-Taan, O.; Arshad, A.; Morgan, B.; Metcalfe, M.S.; Dennison, A.R. The Multifaceted Effects of Omega-3 Polyunsaturated Fatty Acids on the Hallmarks of Cancer. *J. Lipids* **2013**, *2013*, 261247. [[CrossRef](#)]
59. Harris, E. Higher Levels of Omega-3 Fatty Acids Linked to Improved Lung Health. *JAMA* **2023**, *330*, 685. [[CrossRef](#)] [[PubMed](#)]
60. Gerber, M. Omega-3 fatty acids and cancers: A systematic update review of epidemiological studies. *Br. J. Nutr.* **2012**, *107*, S228–S239. [[CrossRef](#)] [[PubMed](#)]
61. Sun, H.; Berquin, I.M.; Owens, R.T.; O’Flaherty, J.T.; Edwards, I.J. Peroxisome proliferator-activated receptor gamma-mediated up-regulation of syndecan-1 by n-3 fatty acids promotes apoptosis of human breast cancer cells. *Cancer Res.* **2008**, *68*, 2912–2919. [[CrossRef](#)] [[PubMed](#)]
62. Gu, Z.; Suburu, J.; Chen, H.; Chen, Y.Q. Mechanisms of omega-3 polyunsaturated fatty acids in prostate cancer prevention. *Biomed. Res. Int.* **2013**, *2013*, 824563. [[CrossRef](#)] [[PubMed](#)]
63. Goncalves, M.D.; Hopkins, B.D.; Cantley, L.C. Dietary Fat and Sugar in Promoting Cancer Development and Progression. *Annu. Rev.* **2019**, *3*, 255–273. [[CrossRef](#)]
64. Avgerinos, K.I.; Spyrou, N.; Mantzoros, C.S.; Dalamaga, M. Obesity and cancer risk: Emerging biological mechanisms and perspectives. *Metabolism* **2019**, *92*, 121–135. [[CrossRef](#)]
65. Toporski, J.; Dieing, T.; Hollricher, O. (Eds.) *Confocal Raman Microscopy*, 2nd ed.; Springer Nature: Berlin/Heidelberg, Germany, 2018; Volume 66, ISBN 3319753789.
66. Brozek-Pluska, B.; Beton, K. Oxidative stress induced by: T BHP in human normal colon cells by label free Raman spectroscopy and imaging. The protective role of natural antioxidants in the form of  $\beta$ -carotene. *RSC Adv.* **2021**, *11*, 16419–16434. [[CrossRef](#)] [[PubMed](#)]
67. Beton, K.; Brozek-Pluska, B. Vitamin C—Protective Role in Oxidative Stress Conditions Induced in Human Normal Colon Cells by Label-Free Raman Spectroscopy and Imaging. *Int. J. Mol. Sci.* **2021**, *22*, 6928. [[CrossRef](#)] [[PubMed](#)]
68. Beton, K.; Brozek-Pluska, B. Biochemistry and Nanomechanical Properties of Human Colon Cells upon Simvastatin, Lovastatin, and Mevastatin Supplementations: Raman Imaging and AFM Studies. *J. Phys. Chem. B* **2022**, *126*, 7088–7103. [[CrossRef](#)] [[PubMed](#)]
69. Surmacki, J.M. Monitoring the effect of therapeutic doses of gamma irradiation on medulloblastoma by Raman spectroscopy. *Anal. Methods* **2020**, *12*, 383–391. [[CrossRef](#)]
70. Beton-Mysur, K.; Brozek-Pluska, B. A new modality for cholesterol impact tracking in colon cancer development—Raman imaging, fluorescence and AFM studies combined with chemometric analysis. *Anal. Methods* **2023**, *15*, 5199–5217. [[CrossRef](#)] [[PubMed](#)]
71. Tolstik, E.; Gongalsky, M.B.; Dierks, J.; Brand, T.; Pernecker, M.; Pervushin, N.V.; Maksutova, D.E.; Gonchar, K.A.; Samsonova, J.V.; Kopeina, G.; et al. Raman and fluorescence micro-spectroscopy applied for the monitoring of sunitinib-loaded porous silicon nanocontainers in cardiac cells. *Front. Pharmacol.* **2022**, *13*, 962763. [[CrossRef](#)] [[PubMed](#)]
72. Voros, C.; Bauer, D.; Migh, E.; Grexa, I.; Vég, A.G.; Szalontai, B.; Castellani, G.; Danka, T.; Dzeroski, S.; Koos, K.; et al. Correlative Fluorescence and Raman Microscopy to Define Mitotic Stages at the Single-Cell Level: Opportunities and Limitations in the AI Era. *Biosensors* **2023**, *13*, 187. [[CrossRef](#)] [[PubMed](#)]
73. Matthäus, C.; Chernenko, T.; Newmark, J.A.; Warner, C.M.; Diem, M. Label-free detection of mitochondrial distribution in cells by nonresonant Raman microspectroscopy. *Biophys. J.* **2007**, *93*, 668–673. [[CrossRef](#)] [[PubMed](#)]
74. Lin, J.; Graziotto, M.E.; Lay, P.A.; New, E.J. A bimodal fluorescence-raman probe for cellular imaging. *Cells* **2021**, *10*, 1699. [[CrossRef](#)] [[PubMed](#)]
75. Van Manen, H.J.; Kraan, Y.M.; Roos, D.; Otto, C. Single-cell Raman and fluorescence microscopy reveal the association of lipid bodies with phagosomes in leukocytes. *Proc. Natl. Acad. Sci. USA* **2005**, *102*, 10159–10164. [[CrossRef](#)] [[PubMed](#)]
76. Tadros, S.; Shukla, S.K.; King, R.J.; Gunda, V.; Vernucci, E.; Abrego, J.; Chaika, N.V.; Yu, F.; Lazenby, A.J.; Berim, L.; et al. De Novo Lipid Synthesis Facilitates Gemcitabine Resistance through Endoplasmic Reticulum Stress in Pancreatic Cancer. *Cancer Res.* **2017**, *77*, 5503–5517. [[CrossRef](#)] [[PubMed](#)]
77. Iwamoto, H.; Abe, M.; Yang, Y.; Cui, D.; Seki, T.; Nakamura, M.; Hosaka, K.; Lim, S.; Wu, J.; He, X.; et al. Cancer Lipid Metabolism Confers Antiangiogenic Drug Resistance. *Cell Metab.* **2018**, *28*, 104–117.e5. [[CrossRef](#)] [[PubMed](#)]
78. Cotte, A.K.; Aires, V.; Fredon, M.; Limagne, E.; Derangère, V.; Thibaudin, M.; Humblin, E.; Scagliarini, A.; De Barros, J.P.P.; Hillon, P.; et al. Lysophosphatidylcholine acyltransferase 2-mediated lipid droplet production supports colorectal cancer chemoresistance. *Nat. Commun.* **2018**, *9*, 322. [[CrossRef](#)] [[PubMed](#)]
79. Bartz, R.; Li, W.H.; Venables, B.; Zehmer, J.K.; Roth, M.R.; Welti, R.; Anderson, R.G.W.; Liu, P.; Chapman, K.D. Lipidomics reveals that adiposomes store ether lipids and mediate phospholipid traffic. *J. Lipid Res.* **2007**, *48*, 837–847. [[CrossRef](#)] [[PubMed](#)]
80. Martin, S.; Parton, R.G. Caveolin, cholesterol, and lipid bodies. *Semin. Cell Dev. Biol.* **2005**, *16*, 163–174. [[CrossRef](#)] [[PubMed](#)]
81. Brasaemle, D.L. Thematic review series: Adipocyte Biology. The perilipin family of structural lipid droplet proteins: Stabilization of lipid droplets and control of lipolysis. *J. Lipid Res.* **2007**, *48*, 2547–2559. [[CrossRef](#)] [[PubMed](#)]

82. Kimmel, A.R.; Brasaemle, D.L.; McAndrews-Hill, M.; Sztalryd, C.; Londos, C. Adoption of PERILIPIN as a unifying nomenclature for the mammalian PAT-family of intracellular lipid storage droplet proteins. *J. Lipid Res.* **2010**, *51*, 468–471. [[CrossRef](#)] [[PubMed](#)]
83. Sun, N.; Zhao, X. Therapeutic Implications of FABP4 in Cancer: An Emerging Target to Tackle Cancer. *Front. Pharmacol.* **2022**, *13*, 948610. [[CrossRef](#)] [[PubMed](#)]
84. Lau, E.; Marques, C.; Pestana, D.; Santoalha, M.; Carvalho, D.; Freitas, P.; Calhau, C. The role of I-FABP as a biomarker of intestinal barrier dysfunction driven by gut microbiota changes in obesity. *Nutr. Metab.* **2016**, *13*, 31. [[CrossRef](#)] [[PubMed](#)]
85. Mahmood, A.; Faisal, M.N.; Khan, J.A.; Muzaffar, H.; Muhammad, F.; Hussain, J.; Aslam, J.; Anwar, H. Association of a high-fat diet with I-FABP as a biomarker of intestinal barrier dysfunction driven by metabolic changes in Wistar rats. *Lipids Health Dis.* **2023**, *22*, 68. [[CrossRef](#)] [[PubMed](#)]
86. Beton, K.; Wysocki, P.; Brozek-Pluska, B. Mevastatin in colon cancer by spectroscopic and microscopic methods—Raman imaging and AFM studies. *Spectrochim. Acta Part A Mol. Biomol. Spectrosc.* **2022**, *270*, 120726. [[CrossRef](#)] [[PubMed](#)]
87. Kopec, M.; Beton-Mysur, K.; Abramczyk, H. Raman imaging and chemometric methods in human normal bronchial and cancer lung cells: Raman biomarkers of lipid reprogramming. *Chem. Phys. Lipids* **2023**, *257*, 105339. [[CrossRef](#)] [[PubMed](#)]
88. Kopec, M.; Beton-Mysur, K. The role of glucose and fructose on lipid droplet metabolism in human normal bronchial and cancer lung cells by Raman spectroscopy. *Chem. Phys. Lipids* **2024**, *259*, 105375. [[CrossRef](#)] [[PubMed](#)]

**Disclaimer/Publisher’s Note:** The statements, opinions and data contained in all publications are solely those of the individual author(s) and contributor(s) and not of MDPI and/or the editor(s). MDPI and/or the editor(s) disclaim responsibility for any injury to people or property resulting from any ideas, methods, instructions or products referred to in the content.